Monte-carlo computation of wall-pressure spectra under turbulent boundary layers for trailing-edge noise prediction.

G. Grasso [1,2]**, P. Jaiswal** [1]**, S. Moreau** [1]
[1] Université de Sherbrooke, Département de Génie Mécanique,
2500 Bd. de l'Université, J1H4X2 Sherbrooke, QC, Canada

[2] Currently affiliated with École Centrale de Lyon, Laboratoire de Mécanique des Fluides et d'Acoustique
36 Avenue Guy de Collongue, 69134 Écully Cedex, France
e-mail: **gabriele.grasso@ec-lyon.fr**

Abstract
The quantification of the spectrum of wall-pressure fluctuations under a turbulent boundary layer has a fundamental role in problems of aerodynamic noise generation and structural vibration. Advanced analytic formulations of the wall-pressure spectrum involve multi-dimensional integrals. The computation of these integral formulations with quadrature methods proves computationally expensive, especially if many flow configurations are taken into account. For this reason, Monte-Carlo methods are used to distribute a predefined number of samples of the integrand function in the integration space and obtain a rapid and accurate estimate of the integral value. This work reviews the expression of the wall-pressure spectrum based on the Poisson equation for pressure fluctuations in a turbulent field and then applies three different Monte-Carlo methods to its computation: the quasi-uniform sampling, the recursive stratified sampling and the importance sampling. The criteria for the choice of the most appropriate Monte-Carlo method are finally discussed.

1 Introduction

The problem of estimating of the spectrum of wall-pressure fluctuations under a turbulent boundary layer arises in the description of aeroacoustic and structural phenomena. From the aeroacoustic point of view, Amiet's model and its extension [1, 30] state that the spectrum of trailing-edge noise emitted by a stationary airfoil is directly proportional to the spectrum of wall-pressure fluctuations generated by the turbulent boundary layer that develops over the airfoil surface. This model is extended to the prediction of noise from low-speed fans [31, 33]. The scattering of the wall-pressure fluctuations at the trailing edge of a blade is one of the main contributions to the broadband noise emitted by subsonic fans [21] and it represents the minimum level of noise emitted by a fan when all leading-edge and tip interactions are removed. Also, the turbulent boundary layer that develops on the external surfaces of air, ground and marine transportation vehicles generates unsteady loads that can excite the underlying structure and propagate towards the interior of the vehicle as sound and vibration [4]. These facts justify the introduction of a fast and accurate prediction of the wall-pressure spectrum in the design process of many different industrial applications. Empirical models of the wall-pressure spectrum scaled with boundary layer variables have been developed most notably by Corcos [9], Chase [6], Schlinker and Amiet [34], Efimtsov [10], Goody [13], Rozenberg *et al.* [32] and Caiazzo *et al.* [4], among others. The advantage of these models consists in their easy mathematical formulation, which poses no problems of numerical implementation. However, they do not provide an explicit correlation between the statistics of the wall pressure and those of the overlying turbulent field. This correlation is formulated in the models based on the Poisson equation of the pressure fluctuations in a turbulent field. The

disadvantage, in this case, is that the formulations of the wall-pressure spectrum resulting from the Poisson equation involve multi-dimensional integrals that require a high computational time when solved with traditional quadrature techniques. This problem was circumvented in the TNO-Blake family of models by making simplifying assumptions on the turbulence statistics that allowed to reduce the dimensionality of the integral formulation (see e.g. Kamruzzaman *et al.* [15] and Bertagnolio *et al.* [2]). However, these assumptions have recently been dismissed as non-physical by Fischer *et al.* [11]. In other works, such as those of Panton and Linebarger [22], Remmler *et al.* [28], Peltier and Hambric [23] and Slama *et al.* [35], the multi-dimensional integral formulations are computed in a reasonable time with different numerical techniques, particularly Monte-Carlo methods and Kriging. This work explores the application of different Monte-Carlo methods to a possible solution of the wall-pressure spectrum based on the Poisson equation considering especially the efficiency and the ease of implementation of these methods.

2 Analytic formulation of the wall-pressure spectrum

2.1 Solution of the Poisson equation

The Poisson equation governing the pressure fluctuations in a turbulent boundary layer derives from the divergence of the incompressible momentum equation, introducing Reynolds decomposition into mean and fluctuating quantities, then subtracting the time-averaged equation. As a result,

$$\frac{1}{\rho}\frac{\partial^2 p}{\partial x_i^2} = \underbrace{-2\frac{\partial u_j}{\partial x_i}\frac{\partial U_i}{\partial x_j}}_{\text{turbulence-mean shear}} \underbrace{-\frac{\partial^2}{\partial x_i \partial x_j}\left(u_i u_j - \overline{u_i u_j}\right)}_{\text{turbulence-turbulence}} \tag{1}$$

where lowercase letters indicate fluctuating quantities and uppercase letters indicate mean quantities. The Laplacian of the unsteady pressure field is equal to the sum of two source terms: the turbulence-mean shear and the turbulence-turbulence interaction. In this work, it is assumed for mathematical simplicity that the main contribution to the wall-pressure spectrum is that of the turbulence-mean shear interaction, according to the estimation made by Kraichnan [16]. However, recent research has highlighted the importance of turbulence-turbulence interaction term on the lower frequency range of the spectrum (see e.g. [35]). Equation (1) is solved for the fluctuating pressure in the domain represented in Fig. 1 using the Neumann boundary condition at the wall and assuming that p vanishes at infinity. The mean flow speed is aligned with the x_1 coordinate and is uniform with respect to x_1 and x_3 As a result, the only significant mean-velocity gradient is in the normal-to-wall direction and the source term of the Poisson equation is reduced to $-2\frac{\partial u_2}{\partial x_1}\frac{\partial U_1}{\partial x_2}$. The turbulent field is considered homogeneous in planes parallel to the wall (having constant x_2 coordinate). Therefore, Eq. (1) can be Fourier-transformed in the x_1 and x_3 directions, yielding the following modified Helmholtz equation:

$$\frac{\partial^2 \hat{p}(\kappa, x_2)}{\partial x_2^2} - \kappa^2\, \hat{p}(\kappa, x_2) = -2\,\rho\,\mathrm{i}\,k_1\,\frac{\partial U_1}{\partial x_2}\hat{u}_2(\kappa, x_2) \tag{2}$$

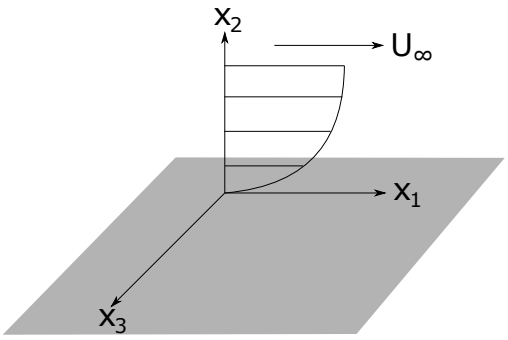

Figure 1: Turbulent boundary layer over an infinite flat plate.

where $(\hat{\cdot})$ represents the double spatial Fourier transform and $\kappa = \sqrt{k_1^2 + k_3^2}$. The solution of Eq. (2) is obtained with the following Green's function (see Gerolymos *et al.* [12] for a complete derivation):

$$G\left(x_2, X_2; \kappa \neq 0\right) = -\frac{\mathrm{e}^{-\kappa|x_2 - X_2|}}{2\kappa} - \frac{\mathrm{e}^{-\kappa(x_2 + X_2)}}{2\kappa} \tag{3}$$

hence the wall pressure is

$$\hat{p}(\kappa, x_2 = 0) = 2\,\mathrm{i}\,\rho \frac{k_1}{\kappa} \int_0^\infty \frac{\partial U_1(X_2)}{\partial x_2} \hat{u}_2(\kappa, X_2) \mathrm{e}^{-\kappa\, X_2} dX_2. \tag{4}$$

The spectrum of wall-pressure fluctuations is obtained by multiplying Eq. (4) by its complex conjugate and taking the ensemble average. The result is integrated over the transverse wavenumber k_3, yielding the streamwise-wavenumber wall-pressure spectrum:

$$\varphi_{pp}(k_1) = 8\rho_0^2 \iiint_0^\infty \frac{k_1^2}{\kappa^2} \mathrm{e}^{-(X_2 + X_2')\kappa} \frac{\partial U_1(X_2)}{\partial x_2} \frac{\partial U_1(X_2')}{\partial x_2} \langle \hat{u}_2(\kappa, X_2) \cdot \hat{u}_2(\kappa, X_2') \rangle dX_2\, dX_2'\, dk_3. \tag{5}$$

According to the hypothesis of 'frozen' convection of the turbulence (see e.g. [22, 11]), the frequency spectrum, $\varphi_{pp}(\omega)$, is a function of the streamwise wavenumber spectrum, $\varphi_{pp}(k_1)$, as $\varphi_{pp}(\omega) = \varphi_{pp}(k_1 \rightarrow \omega/U_c)/U_c$.

2.2 Cross-spectrum of vertical velocity fluctuations

The vertical velocity fluctuation statistics that appear in Eq. (5) is modeled with the following relationship:

$$\langle \hat{u}_2(\kappa, X_2) \cdot \hat{u}_2(\kappa, X_2') \rangle = \sqrt{\overline{u_2^2(X_2)}\; \overline{u_2^2(X_2')}}\, S_{22}(\kappa, X_2, X_2') \tag{6}$$

where S_{22} is the normalized cross-spectrum of u_2. The analytic expression of S_{22} is derived as follows.

The normalized vertical velocity correlation coefficient is defined for a homogeneous turbulent field as

$$R_{22}\left(r_1, r_2, r_3\right) = F\left(r\right) + \frac{r_1^2 + r_3^2}{2r} F'\left(r\right) \tag{7}$$

where $r = \sqrt{r1^2 + r_2^2 + r_3^2}$ and $F(r)$ is the longitudinal correlation function. For the present calculations, the correlation function is assumed to be a Gaussian:

$$F\left(r\right) = \exp\left(-\frac{r^2}{\Lambda_g^2}\right). \tag{8}$$

where Λ_g is an integral length scale. Other functions can be chosen to represent $F(r)$ (see [36] for an extensive discussion) but the Gaussian has the advantage of providing a simple closed-form solution of the cross-spectrum, S_{22}, and is therefore well-suited for numerical validation. The cross-spectrum of vertical velocity fluctuations is defined as the real part of the double spatial Fourier transform of R_{22} in the streamwise and transverse directions:

$$S_{22}(\kappa, X_2, X_2') = \frac{1}{4\pi^2} \int_0^\infty \int_0^{2\pi} R_{22} \cos(k_1\, r_{1,3} \cos(\theta)) \cos(k_3\, r_{1,3} \sin(\theta)) d\theta dr_{1,3} \tag{9}$$

where the polar coordinates $r_{1,3} = \sqrt{r_1^2 + r_3^2}$ and $\theta = \arcsin(r_3/r_1)$ have been used. It can be shown that the integral in $d\theta$ of Eq. (9) has an analytic solution, which yields

$$S_{22}(\kappa, X_2, X_2') = \frac{1}{2\pi} \int_0^\infty R_{22} J_0\left(r_{1,3}\, \kappa\right) r_{1,3} dr_{1,3} \tag{10}$$

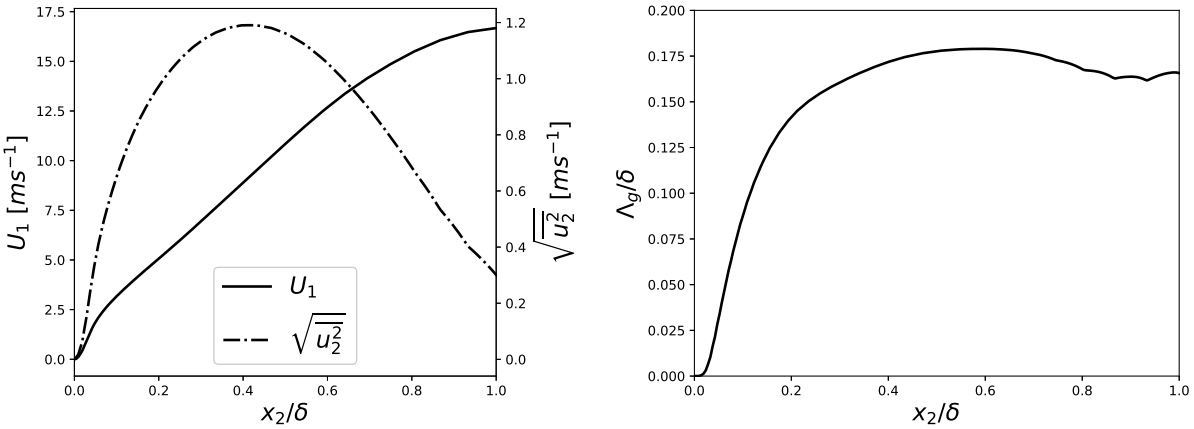

(a) Mean velocity and turbulence intensity

(b) Integral length scale

Figure 2: Boundary layer profiles of the CD airfoil used as input to the wall-pressure spectrum calculation.

where J_0 is the Bessel function of the first kind of order 0. The last equation states that the cross-spectrum of u_2 is the Hankel transform of R_{22} in the $r_{1,3}$ direction. Finally, the solution of the integral of Eq. (10) yields

$$S_{22}(\kappa, X_2, X_2') = \frac{1}{2\pi} \mathrm{e}^{-\frac{(X_2 - X_2')^2}{\Lambda_g^2}} \frac{\kappa^2 \Lambda_g^4}{8} \mathrm{e}^{-\frac{\kappa^2 \Lambda_g^2}{4}} \tag{11}$$

where the X_2 and X_2' coordinates are written explicitly due to the inhomogeneity of the turbulence in the normal-to-wall direction. The introduction of Eqs. (9), (10) or (11) in Eq. (5), although formally indifferent, yields a five-dimensional, a four-dimensional or a three-dimensional integral formulation of the wall-pressure spectrum, respectively. The computation of the wall-pressure spectrum with classical quadrature techniques requires an amount of computational time that increases with the number of dimensions in the integral formulation. However, this mathematical model provides a useful test case to assess the efficiency of Monte-Carlo methods working with a pre-defined number of samples of integrand functions of increasing complexity.

3 Test Case

The application case for the computation of wall-pressure spectra is a controlled-diffusion (CD) airfoil for which it exists a large experimental and numerical database [19, 33]. The present profile corresponds to the mid-span section of the H380EC1 fan blade [18]. It has a 4% relative thickness and a camber angle of 12^o. The airfoil chord length is $c = 0.1356$ m. It is set at a geometrical angle of attack of $\alpha_w = 8^o$. The reference velocity is $U_0 = 30$ m/s, defining a Reynolds number based on the airfoil chord length $Re_c = 2.8 \cdot 10^5$. A LES and a RANS simulation of the flow over the CD airfoil have been performed with OpenFOAM [7]. The turbulence model selected for the RANS simulation was the k-ω SST. The boundary-layer quantities necessary for the wall-pressure spectrum prediction have been extracted from the RANS simulation using BATMAN, the VKI in-house code for noise prediction. The results of the extraction are depicted in Fig. 3, where the x_2 coordinate is normalized by the boundary layer thickness, δ. Details of the computation of $\sqrt{\overline{u_2^2}}$ and Λ_g from a RANS simulation are given in the paper of Remmler *et al.* [28]. The wall-pressure spectrum directly computed from the LES simulation is retained throughout this study for comparison with the predicted spectra.

The frequency wall-pressure spectra presented in the following figures are computed from the corresponding wavenumber spectra given by Eq. (5). The convective speed of pressure fluctuations over the blade surface, U_c, is supposed to be independent of the wavenumber and equal to 70% of the reference velocity U_0. This is a common value for turbulent boundary layer convection velocity (see [29, p. 50] and [20, Tab. 1]). The

treatment of length scale anisotropy in the turbulent field and of its effect on S_{22} is described in detail by Remmler [28].

4 Monte-Carlo methods

Various numerical schemes have been devised in the past for the numerical calculation of multi-dimensional integral, and the reader is referred to [26] for a brief overview. However most of the classical quadrature schemes can be computationally demanding if the dimension of the integral is high [17]. As an estimate if 100 points are required for calculation of a single independent variable, then the required cost for N dimensional integral using a classical quadrature technique would be 100^N. Furthermore this would be the cost for a single streamwise-wavenumber calculation, in principle then if one wants to calculate the pressure spectra at M different streamwise wavenumber this cost will go upto $M \times 100^N$. This can be computationally heavy if N is large, even by current state of the art computer. Whereas as noted if we want to estimate wall pressure spectra from a pre-design perspective where a hundred of test cases are to be tested and as such a large computational cost for a single case can prove to be detrimental. With this in mind the Monte-Carlo method for numerical integration has been used, which is computationally much cheaper and can converge with just a moderate $3000 - 5000$ iterations per streamwise wavenumber as noted previously by [22], [17] and [28] using a similar formulation for the calculation of wall-pressure spectra.

4.1 Quasi uniform sampling

The simplest way to integrate a generic function $f : \mathbb{R}^n \to \mathbb{R}$ with Monte-Carlo schemes is to generate N random vectors, $\mathbf{x}_i$, over the integration domain. Following the review made by Press and Farrar [25], we can define the estimator of f, which is obtained by calculating the mean of the N randomly sampled function values:

$$\langle \tilde{f} \rangle = \frac{1}{N} \sum_{i=1}^{N} f(\mathbf{x}_i). \tag{12}$$

An indication of the error of the Monte-Carlo integration is given by the square root of the variance of the estimator, $\mathrm{Var}(\langle \tilde{f} \rangle)$. The variance of the estimator, in its turn, is related to the variance of the function as

$$\mathrm{Var}(\langle \tilde{f} \rangle) = \frac{\mathrm{Var}(f)}{N} \tag{13}$$

so that the following asymptotic relation holds for the error of the estimation:

$$\epsilon = \mathcal{O}\left(\frac{\sigma}{\sqrt{N}}\right) \tag{14}$$

where $\sigma = \sqrt{\mathrm{Var}(f)}$. However it is a known fact that generating random numbers using a deterministic computer is not possible, since a deterministic computer will always generate the same output if the starting conditions and inputs are the same. On the other hand one can generate so called pseudo random numbers using built-in libraries. However such random number generators are based on recurrence relations, and as such they would repeat afterwards. Although, there exists a random number generators which can take care of this problem of short-periods [26], nevertheless variance reduction obtained by generating pseudo-random sequence is quite slow and it converges with a rate of $N^{-1/2}$ [26], where N is the number of samples. To avoid this [22] and [17] used quasi-random sequences to sample the integral, this can improve the rate of convergence of the integral to N^{-1} under certain boundary conditions [26]. Thus for our test cases we use the Sobol sequence for generating Quasi-Random (QR) numbers using the function $sobseq$ taken directly from [27].

4.2 Recursive stratified sampling/Miser algorithm

A different technique, the recursive stratified sampling, has been developed by Press and Farrar and implemented in the MISER algorithm [25]. The fundamental idea is to divide the integration region V into two equal and disjoint subvolumes, a and b, and sample them with N_a and $N_b = N - N_a$ uniformly distributed points, respectively. Then, a new estimator of $\langle f \rangle$ is defined as

$$\langle \tilde{f} \rangle' = \frac{1}{2}\left(\langle \tilde{f} \rangle_a + \langle \tilde{f} \rangle_b\right) \tag{15}$$

where the $\langle \tilde{f} \rangle_{a,b}$ terms are computed according to Eq. (12). The variance of the newly defined estimator is

$$\text{Var}\left(\langle \tilde{f} \rangle'\right) = \frac{1}{4}\left(\frac{\text{Var}_a(f)}{N_a} + \frac{\text{Var}_b(f)}{N - N_a}\right) \tag{16}$$

which is minimized when

$$\frac{N_a}{N} = \frac{\sigma_a}{\sigma_a + \sigma_b}. \tag{17}$$

In case N_a satisfies the previous equation, the variance of the function mean estimator is

$$\text{Var}\left(\langle \tilde{f} \rangle'\right) = \frac{(\sigma_a + \sigma_b)^2}{4N}. \tag{18}$$

The advantage of this method is that Var $\left(\langle \tilde{f} \rangle'\right)$ is never larger than the variance of the estimator computed in the general Monte-Carlo method, defined in Eq. (13). The stratified sampling can be applied recursively to solve high-dimensional problems; the details of this procedure are given in [25]. The MISER algorithm is available in the `Scikit-Monaco` package for Python [3].

4.3 Importance sampling

Another way to accelerate the convergence by reducing variance the technique of Importance Sampling (IS) method can be used as done previously by [22], [17] and [28]. The method of importance sampling is based on the simple idea that by introducing a change in variable the function could be made flatter in the new co-ordinate system and hence fewer samples would be required to reach convergence. In fact if the function is flat just a single sample would be required.

Mathematically importance sampling can be defined as

$$E_f[h(X)] = \int_X h(x)g(x)dx \tag{19}$$

In the above equation we seek to determine the expectation E of function $h(x)$ under the Probability Density Function (PDF) $g(x)$.

Generally we need to either find the PDF $g(x)$ that mimics the function $h(x)$ in case if such a function is not present intrinsically in the integral. Then from there on samples could be drawn from the function $g(x)$ using the technique known as Inverse transform sampling.

The algorithm for inverse transform sampling can be summarized as-

1) Determine the PDF function $g(x)$ which "resembles" $h(x)$.

2) Determine its Cumulative Distribution Function (CDF) $u(x)$.

3) Find its inverse $u^{-1}(x)$ either numerically or analytically.

4) Generate uniformly distributed random numbers using Sobol sequence and plug it to $u^{-1}(x)$, this would generate random number based on the PDF $g(x)$.

5) Solve Eq. (19).

Before importance sampling was realised, the Quintuple Integrals was further simplified in order to facilitate its numerical implementation. Firstly all the length scales in the equation were normalised using δ (the boundary layer thickness) as follows : $k = k\delta$, $x_2 = x_2/\delta$, $\lambda_g = \lambda_g/\delta$ and $r = r/\delta$. Secondly the integral is split in two different terms $\varphi(K_1) = I_1 - I_2$ as was done by [22],with I_1 :

$$\left\{ \begin{array}{l} I_1 = \dfrac{2\alpha {k_1}^2 \rho^2}{\pi^2} \displaystyle\int_0^{2\pi} \int_0^{\infty} \int_0^1 \int_0^1 \int_0^{\infty} \frac{1}{\kappa^2} \times \mathrm{e}^{(-\kappa(X_2{}' + X_2))} \ldots \\ \sqrt{\overline{u_2^2(X_2)}\,\overline{u_2^2(X_2')}}\,\delta^3 \times \left[(r) \times \exp\left(- \left(\dfrac{r^2 + (X_2 - X_2{}')^2}{{\Lambda_g}^2} \right) \right) \right] \\ \dfrac{\partial U}{\partial x_2} \dfrac{\partial U}{\partial x_2{}'} \cos(k_1 \alpha r \cos\theta) \cos(k_3 r \sin\theta) d\theta dr dX_2 dX_2{}' dk_3 \end{array} \right\} \tag{20}$$

and I_2 :

$$\left\{ \begin{array}{l} I_2 = \dfrac{2\alpha {k_1}^2 \rho^2}{\pi^2} \displaystyle\int_0^{2\pi} \int_0^{\infty} \int_0^1 \int_0^1 \int_0^{\infty} \frac{1}{\kappa^2} \times \mathrm{e}^{(-\kappa(X_2{}' + X_2))} \ldots \\ \sqrt{\overline{u_2^2(X_2)}\,\overline{u_2^2(X_2')}}\,\delta^3 \times \left[\left(\dfrac{r^3}{{\Lambda_g}^2} \right) \times \exp\left(- \left(\dfrac{r^2 + (X_2 - X_2{}')^2}{{\Lambda_g}^2} \right) \right) \right] \\ \dfrac{\partial U}{\partial x_2} \dfrac{\partial U}{\partial x_2{}'} \cos(k_1 \alpha r \cos\theta) \cos(k_3 r \sin\theta) d\theta dr dX_2 dX_2{}' dk_3 \end{array} \right\} \tag{21}$$

For the variance reduction for the variables x_2 and $x_2{}'$ a normal distribution is used,while tailored design of the PDF's used for these variables are driven from previous observations on wall-pressure spectra. In particular the design is motivated by the fact that high frequency and high wave-number contributions comes from the inner part of boundary layer, while at low wavenumber contributions are usually due to external parts of the boundary layer [5]. Secondly the higher frequency contributions are much more localised or stratified, while low frequency contributions are more spread out [22]. Lastly the inner most part of viscous sub-layer part of the boundary layer will have very low contribution towards overall spectra due to the fact that vertical velocity fluctuations tend to zero. By taking these considerations into account, the Eq. (22) is devised :

$$g(x) = 2 * \sqrt{(b * k_1)} \times \left[\frac{\left[\exp[-(b * k_1 * (x - \frac{ah}{k_1})^2)] \right]}{\left[\sqrt{\pi} [\mathrm{erf}(\frac{a * \sqrt{b} * h}{\sqrt{k_1}}) + \mathrm{erf}(\frac{\sqrt{b}(-a * h + k_1)}{\sqrt{k_1}})] \right]} \right] \tag{22}$$

where erf is the Error function. Here K_1, corresponds to the streamwise wavenumber, while b, a and h are empirical constants, to accomplish the above mentioned objectives. The CDF of Eq. (22) turns out to be fairly complicated such that it cannot be analytically inverted. To do this Brent's method of finding the root was used [27]. Brent's method of finding root is a hybrid method [26], and it uses a combination of bisection method, the secant method and inverse quadratic interpolation root , to find roots. An advantage is that, such a method compared to other classical root finding method such as the method of false position used by [17], it performs better even when the function is not smooth near the root [26].

The variance reduction for the variable $\tilde{k}_3$ was realised by using the following PDF:

$$g(x) = (a \times \exp(-(x^2 \times a^2/4)))/(\sqrt{(\pi)} * \mathrm{erf} * (ad/2)) \tag{23}$$

where d is the upper limit of integration for the variable $\tilde{k}_3$. Finally a in Eq.(23) is meant to emulate the behaviour of λ_g. The PDF used for variance reduction for the variable r in the integral I_1 Eq. (20) and I_2 Eq. (21), have following form respectively.

$$g(x) = \left[2 * x \frac{\left[\exp(-[\frac{x^2+c^2}{L^2}])\right]}{L^2 \exp[-(\frac{c^2}{L^2})]}\right] \tag{24}$$

$$g(x) = \left[2 * x^3 \frac{\left[\exp(-[\frac{x^2+c^2}{L^2}])\right]}{L^2\left[L^2 \times \exp[-\frac{c^2}{L^2}]\right]}\right] \tag{25}$$

Here the variable c is meant to emulate $[x_2 - x_2{}']$. L mimics Λ_g.

Lastly for the variable θ, the variable selection turns out to be quite tricky; this was the reason why [22], [17] used a uniform distribution to sample it. However, we know that the variable θ behaves like a Bessel function of the first kind of order 1. But due to its oscillatory behaviour we cannot construct a PDF directly. Although there is an option to take the absolute value of the function and then create the PDF in a piecewise fashion. However this would be a complicated step to implement numerically. A more realistic way is then to note that a Bessel function decreases with a rate of $1/\sqrt{x}$. And since this function is simple enough, it is more amenable to mathematical and programming procedure involved. Hence the PDF chosen for variance reduction for the variable θ is :

$$g(x) = \frac{1}{2 \times \sqrt{(x * 2 * \pi)}} \tag{26}$$

5 Adaptive Quadrature method

The techniques described in section 6 have already been used in the past by numerous other authors e.g. [22], [17] and more recently by [28] to calculate the wall-pressure spectra. However due to mathematical complexities and high computational cost associated with performing a numerical quadrature scheme, a direct one to one comparison between MC integration scheme and a quadrature scheme has not been realized yet in the context of wall-pressure spectra calculations. This is important since while performing such a stochastic integration scheme a notion of absolute or relative accuracy cannot be devised. Rather only the variance of the integral can be controlled. Hence the notion of variance reduction exists which was discussed in the sections before. Be it as it may, this does not let one to determine the accuracy of results. Hence although [22] have extensively tested reduction in variance while using such a stochastic scheme, it is unknown if there solution did or did not converge to the right answer. Also as discussed in section 6 that variance reduction while using importance sampling scheme (as was employed by all the previous authors [22], [17] and [28]) is very sensitive to the choice of distribution function. A wrong choice of distribution function while may lead to an efficient reduction in variance it can nevertheless certainly make the solution digress from the correct solution. In order to quantify the relative accuracy of the calculated wall-pressure spectra using various Monte-Carlo schemes we employ an adaptive quadrature schemes wherein relative errors can be set a-priori, which then can be considered as the reference. This indirect method provides an alternative way of quantifying errors, in a relative sense. The method used for adaptive quadrature integration scheme was tplquad, which can be simply imported from the Python inbuilt scipy.integrate library [14]. For the case where limits of integration are finite, this package uses Clenshaw-Curtis method of cubature [24]. The way it is implemented in Python, user has a choice of either specifying absolute or relative accuracy or both. Since the value of the integral being calculated is below the default absolute accuracy limit, this value was modified and ascribed an arbitrary low value that cannot be achieved numerically, and the relative accuracy was set as 0.9×10^{-3}. This forces the integral to converge within the prescribed limits of relative accuracy.

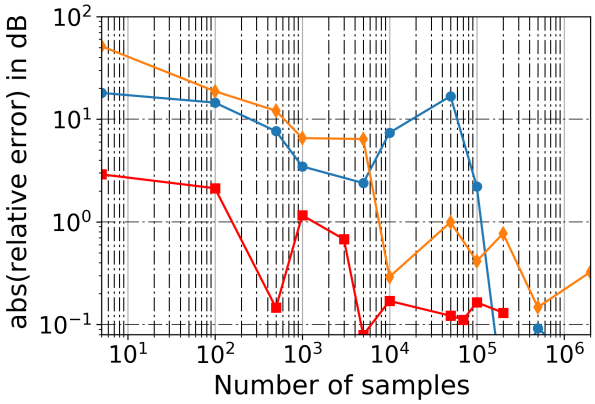

Figure 3: Convergence of different integration schemes Legends: MC MISER sampling error calculated at lowest frequency ; MC QR sampling error calculated at lowest frequency; MC IS sampling error calculated at highest frequency

6 Compare the convergence of the three algorithms against the quadrature scheme

Methods discussed above for the calculation of wall pressure spectra were tested and comparisons are presented in this section. All the cases were run on a Intel(R) Xeon(R) CPU $E3-1270$ v5 Linux workstation with memory base frequency of 3.60GHz and 8 processors with a total of 32 Gb of ram and 8 Mb cache memory. It is worth noting that while both the Monte-Carlo schemes (the importance sampling and the Quasi-random sampling) were written in $Fortran90$, the MISER algorithm and adaptive quadrature scheme-$tplquad$ are both standard Python libraries. Moreover the $Fortran90$ codes were not parallelized while MISER algorithm is. Therefore the differences in time taken for calculation of wall pressure spectra do not necessarily correlate with efficiency of the scheme. Nevertheless time taken for calculation remains an important metric especially, if this method for wall-pressure calculations has to be used in conjunction with pre-design. For the 3 dimensional Quasi-random sampling the rate of calculation per sample was found to be around 2.9×10^{-5} seconds. 2 million samples were calculated under 1 minute. For 4 and 5 dimensional Quasi-random sampling the calculation rate was found to be around 4.4×10^{-5} seconds and 1.4×10^{-4} seconds respectively. Whereas due to inherent complexity involved in coding and number of supplementary operations required in the case of importance sampling meant that the solver takes longer to calculate integral for a single sample. For example in case of 5D integral using importance sampling scheme takes 0.9×10^{-3} seconds to calculate a single sample. For a 4 dimensional integral the cost of calculating integral is about 0.84×10^{-3} seconds, while for a 3 dimensional integral it costs about 1.02×10^{-3} seconds for a single sample. The differences in the latter results are most probably caused by an optimization issue with the code. In any case, it is an order of magnitude higher compared with the time taken by Quasi-random sampling technique for an integral of 5 dimensions. Lastly the [MISER or the Recursive stratified sampling] [25], as implemented in Python [3] is parallelized, hence the time taken per sample is no longer linear as function of sample. The rate is now a function of number of Monte-Carlo samples. For comparison purposes we only report that it takes about 7 minutes to perform Recursive stratified sampling technique on 2 million samples, irrespective of the dimension of the integral. Finally, one should now compare the time taken by these stochastic integration techniques against deterministic quadrature technique. The time taken for the $tplquad$ solution is about 1 hour and 15 minutes with the errors specified. This then clearly shows that Monte-Carlo schemes are several orders of magnitude faster then adaptive quadrature method for integration and it also gives reasonable estimate on a dB scale. Also the Monte-Carlo Quasi-random sampling scheme for integration converges very quickly at higher frequencies while the variance at low frequency is relatively high, this has also been reported in a previous study by Christophe *et al.* [8]. Figure 3 compares the convergence of

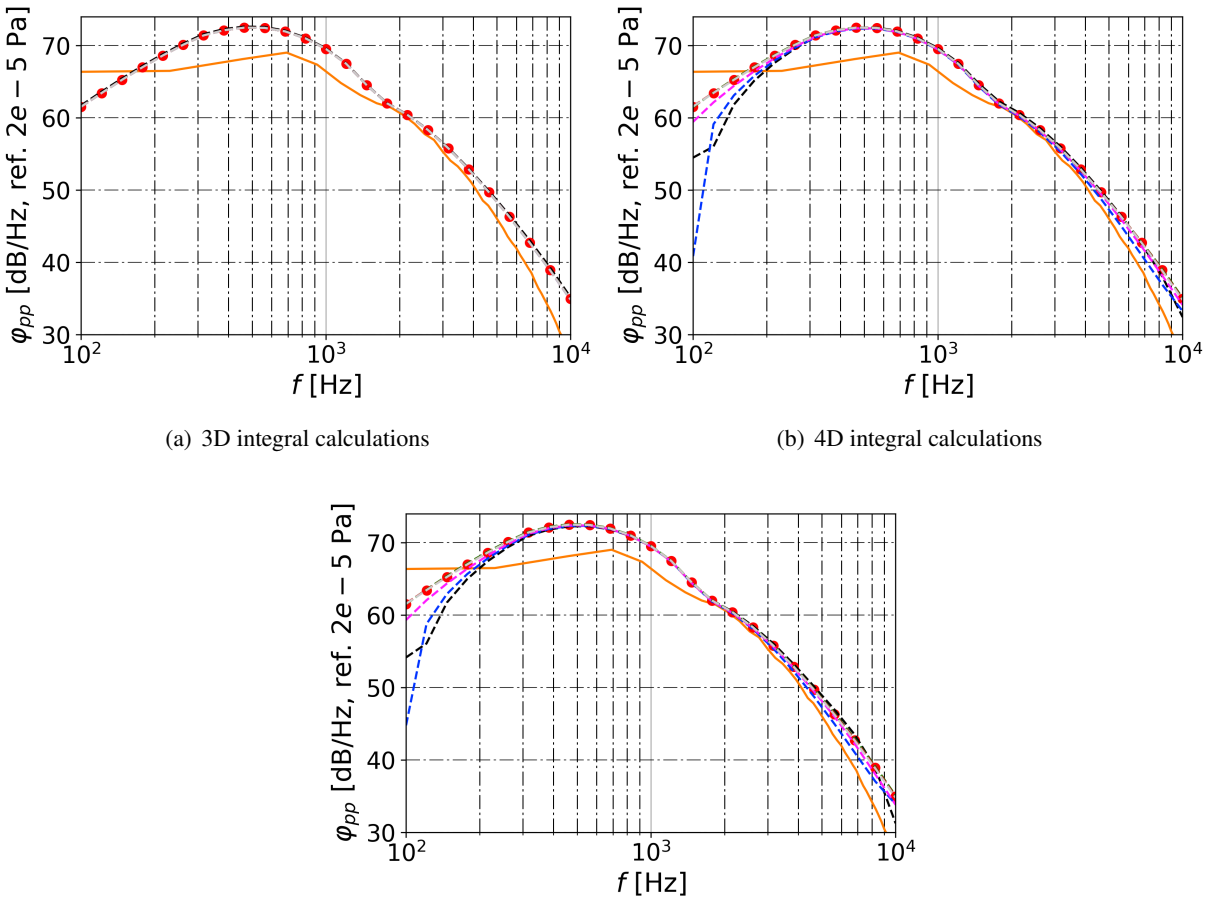

(a) 3D integral calculations

(b) 4D integral calculations

(c) 5D integral calculations

Figure 4: Wall pressure spectra at $x_1/chord = 0.98$ for MC QR sampling. Legends: ● Quadrature solution using tplquad ; —— Reference LES ; - - - With 10k samples; - - - With 50k samples ; - - - With 100k samples ; - - - With 200 k samples ; - - - With 500k samples ; - - - With 2M samples

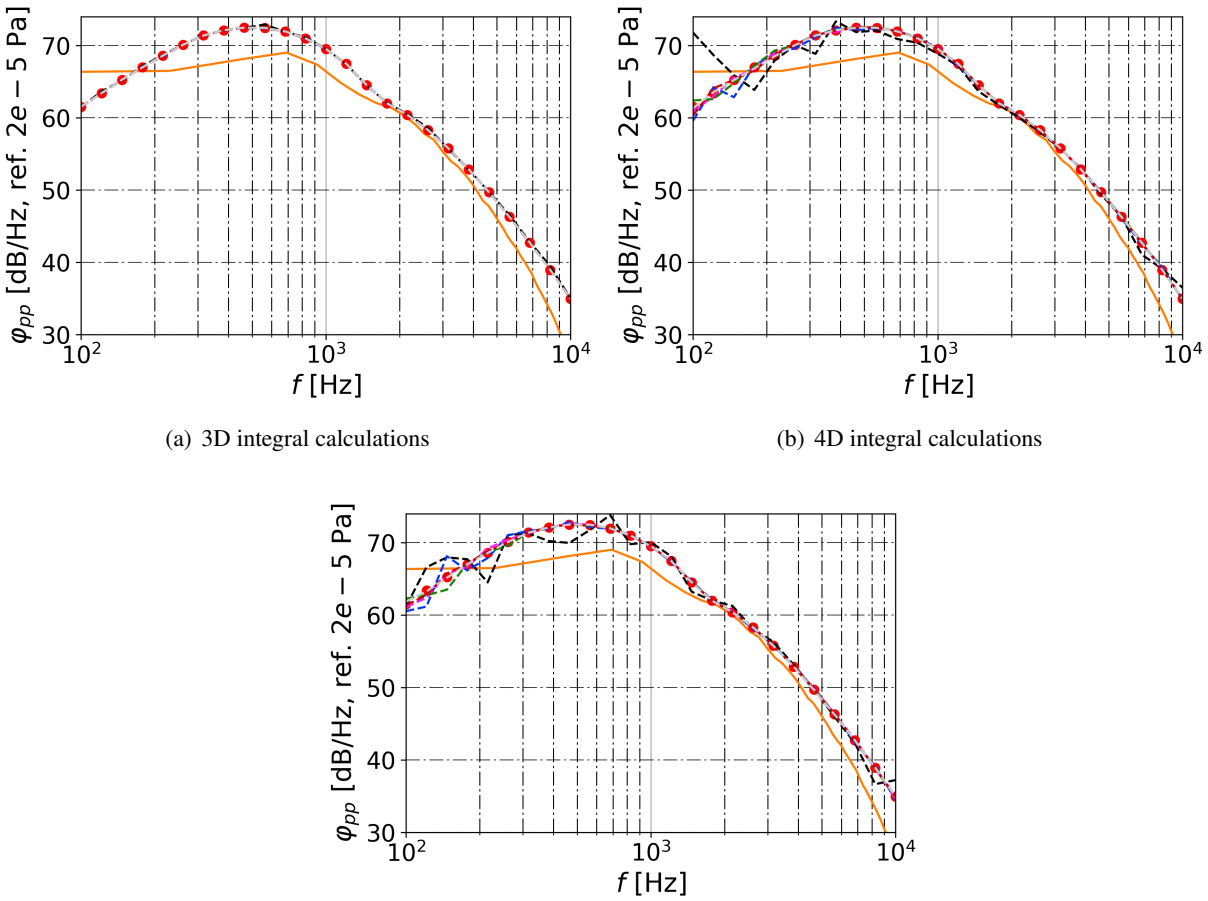

(a) 3D integral calculations

(b) 4D integral calculations

(c) 5D integral calculations

Figure 5: Wall pressure spectra at $x_1/chord = 0.98$ for MC MISER. Legends: ● Quadrature solution using tplquad ; —— Reference LES ; - - - With 10k samples; - - - With 50k samples ; - - - With 100k samples ; - - - With 200k samples ; - - - With 500k samples ; - - - With 2 M samples

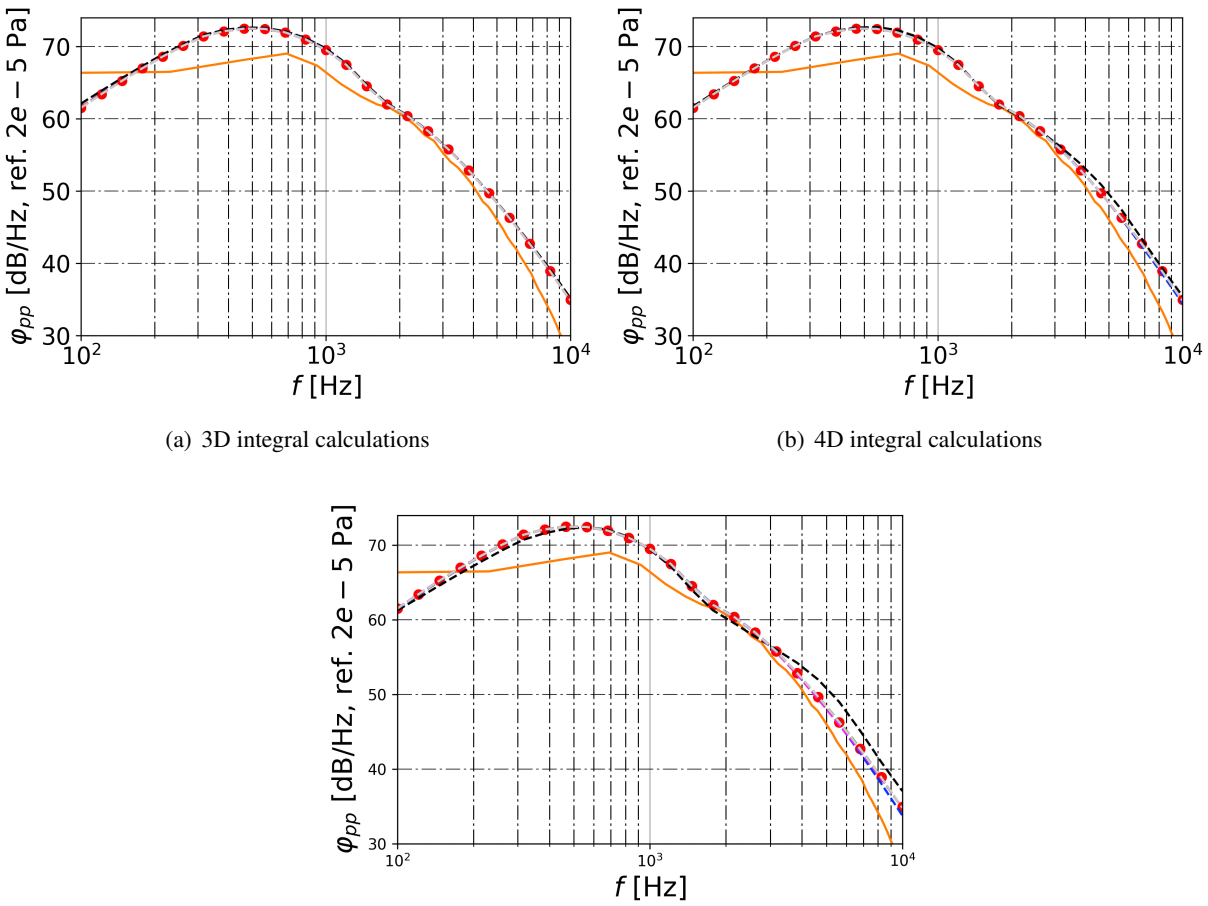

(a) 3D integral calculations

(b) 4D integral calculations

(c) 5D integral calculations

Figure 6: Wall pressure spectra at $x_1/chord = 0.98$ for MC IS. Legends: ● Quadrature solution using tplquad ; — Reference LES ; - - - With 100 samples; - - - With 1k samples ; - - - With 5k samples ; - - - With 10k samples ; - - - With 100k samples ; - - - With 200 k samples

the three Monte-Carlo methods to the adaptive quadratures solution with the number of samples for a given frequency. In this case, the advantage of importance sampling appears clearly.

The wall-pressure spectra computed with the three Monte-Carlo methods are presented in Figs. 4 to 6. First, it can be noticed that the Quasi-Random sampling (Fig. 4) and the MISER algorithm (Fig. 5) exhibit a similar behavior. In fact, for the 3D integration test both algorithms provide a solution consistent with that of the adaptive quadratures already at the lowest number of samples of the integrand function. When the dimensions of the integral formulation are increased to 4 and 5, both methods require a larger number of samples (the order of 10^5) to converge to the reference solution in the lower frequency range. The slow statistical convergence at low frequencies of a Monte-Carlo method for the computation of the wall-pressure spectrum based on the Poisson equation was already noticed by Christophe *et al.* [8]. In their work, a slightly different formulation of the turbulence cross-spectrum was used, assuming an exponential longitudinal correlation function instead of a Gaussian, following [17] and [22]. Figure 6 presents the results of the application of the Importance sampling method to the three integral formulations. These plots demonstrate the advantage of using a variance-reduction method tailored to the integrand function: a converged solution can be obtained with a lower number of samples than the previous Monte-Carlo methods irrespective of the number of dimensions of the integral.

7 Conclusions and future work

This work has presented the application of three different Monte-Carlo techniques to integrand functions of increasing complexity that are of great interest in the study of sound and vibration generated by turbulent boundary layers. The methods taken into account range from the simplest application of Monte-Carlo integration, in which the samples of the function are selected quasi-randomly, to a technique tailored to the specific problem, such as Importance sampling. The results of the convergence tests presented in Sec. 6 show that the Importance sampling technique requires a significantly lower amount of computational resources to obtain the same result as the Quasi-random sampling or the MISER algorithm. However, the drawback of the Importance sampling technique is the necessity of developing an algorithm tailored to every given problem of integration. The MISER algorithm, on the contrary, can be applied to a very wide range of functions of any dimension and is efficiently parallelized in Python and therefore it constitutes a valid alternative.

The analytic modeling of wall-pressure spectra under turbulent boundary layers will be extended in future works to the use of different longitudinal correlation functions of the turbulent field, which are possibly not as mathematically convenient as the Gaussian (see [36]). Furthermore, the effect of the turbulence-turbulence interaction source term in the Poisson equation can be taken into account, leading to six-dimensional integral formulations, as shown in [23] and [35]. In light of these analytic developments, the use of efficient integration techniques illustrated in this paper will be all the more necessary.

Acknowledgements

The Authors gratefully acknowledge the support of the European Union under the project SCONE (grant agreement no. 755543) and the Canadian NSERC Discovery Grant (no: RGPIN-2014-04111).

References

[1] R. K. Amiet, *Noise due to turbulent flow past a trailing edge*, Journal of Sound and Vibration **4** (1976), no. 3.

[2] F. Bertagnolio, A. Fischer, and W. J. Zhu, *Tuning of turbulent boundary layer anisotropy for improved surface pressure and trailing-edge noise modeling*, Journal of Sound and Vibration **333** (2014), 991–1010.

[3] P. Buignon, *Scikit-monaco documentation*, `http://scikit-monaco.readthedocs.io/en/latest/`, 2013.

[4] A. Caiazzo, D'Amico R., and W. Desmet, *A generalized corcos model for modelling turbulent boundary layer wall pressure fluctuations*, Journal of Sound and Vibration **372** (2016), 192–210.

[5] Peter A Chang III, *Relationships between turbulent wall pressure and velocity field sources*, Ph.D. thesis, 1998.

[6] D. M. Chase, *Modeling the wavevector-frequency spectrum of turbulent boundary layer wall pressure*, Journal of Sound and Vibration **70** (1980), no. 1, 29–67.

[7] J. Christophe, *Private communication*.

[8] J Christophe, S Moreau, CW Hamman, JAS Witteveen, and G Iaccarino, *Uncertainty quantification for the trailing-edge noise of a controlled-diffusion airfoil*, AIAA Journal **53** (2014), no. 1, 42–54.

[9] G. M. Corcos, *The structure of the turbulent pressure field in boundary-layer flows*, Journal of Fluid Mechanics **18** (1964), 353–379.

[10] B. M. Efimtsov, *Characteristics of the field of turbulent wall pressure fluctuations at large reynolds numbers*, Soviet Physics Acoustical **28** (1982), no. 4, 289–292.

[11] A. Fischer, F. Bertagnolio, and H. Aa. Madsen, *Improvement of tno type trailing edge noise models*, European Journal of Mechanics B/Fluids (2017), no. 61, 255–262.

[12] G. A. Gerolymos, D. Sénéchal, and I. Vallet, *Wall effects on pressure fluctuations in turbulent channel flow*, Journal of Fluid Mechanics **720** (2013), 15–65.

[13] M. Goody, *Empirical spectral model of surface pressure fluctuations*, AIAA Journal **42** (2004), no. 9, 1788–1794.

[14] Eric Jones, Travis Oliphant, Pearu Peterson, et al., *SciPy: Open source scientific tools for Python*, 2001–, [Online; accessed May 27th 2018].

[15] M. Kamruzzaman, Th. Lutz, W. Würz, W. Z. Shen, W. J. Zhu, M O. L. Hansen, F. Bertagnolio, and H. Aa. Madsen, *Validations and improvements of airfoil trailing-edge noise prediction models using detailed experimental data*, Wind Energy **15** (2012), 45–61.

[16] R. C. Kraichnan, *Pressure fluctuations in turbulent flow over a flat plate*, Journal of the Acoustical Society of America **28** (1956), no. 3, 378–390.

[17] J. H. Linebarger, *Computation of the spectra of turbulent boundary layer surface-pressure fluctuations*, Ph.D. thesis, Oklahoma State University, 1972.

[18] S. Magne, S. Moreau, and A. Berry, *Subharmonic tonal noise from backflow vortices radiated by a low-speed ring fan in uniform inlet flow*, Journal of the Acoustical Society of America **137** (2015), no. 1, 228–237.

[19] S. Moreau, *Symposium on the cd airfoil - introduction*, `https://www.researchgate.net/publication/304582435_CD-day_S-Moreau`, 2016.

[20] S. Moreau and M. Roger, *Effect of airfoil aerodynamic load on trailing edge noise*, AIAA Journal **43** (2005), no. 1, 41–52.

[21] Stephane Moreau and Michel Roger, *Competing broadband noise mechanisms in low-speed axial fans*, AIAA journal **45** (2007), no. 1, 48–57.

[22] R. L. Panton and J. H. Linebarger, *Wall Pressure Spectra Calculations for Equilibrium Boundary Layers*, J. Fluid Mech. **65** (1974), no. 02, 261–287.

[23] L. J. Peltier and S. A. Hambric, *Estimating turbulent-boundary-layer wall-pressure spectra from cfd rans solutions*, Journal of Fluids and Structures **23** (2007), 920–937.

[24] Robert Piessens, Elise de Doncker-Kapenga, Christoph W Überhuber, and David K Kahaner, *Quadpack: a subroutine package for automatic integration*, vol. 1, Springer Science & Business Media, 2012.

[25] W. H. Press and G. R. Farrar, *Recursive stratified sampling for multidimensional monte carlo integration*, Computers in Physics **190** (1990), no. 4.

[26] W. H. Press, S. A. Teukolsky, W. T. Vetterling, and B. P. Flannery, *Numerical recipes in fortran 77. vol. 1*, Press Syndicate of the University of Cambridge, New York, NY, 1992.

[27] William H Press, Saul A Teukolsky, William T Vetterling, Brian P Flannery, and M Metcalf, *Numerical recipes in fortran 90: Volume 2, volume 2 of fortran numerical recipes: The art of parallel scientific computing*, Cambridge University Press, 1996.

[28] S. Remmler, J. Christophe, J. Anthoine, and S. Moreau, *Computation of wall-pressure spectra from steady flow data for noise prediction*, AIAA Journal **48** (2010), no. 9, 1997–2007.

[29] M. Roger and S. Moreau, *Broadband self noise from loaded fan blades*, AIAA Journal **42** (2004), no. 3, 536–544.

[30] M. Roger and S. Moreau, *Back-scattering correction and further extensions of Amiet's trailing-edge noise model. Part 1: Theory*, Journal of Sound and Vibration **286** (2005), no. 3, 477–506.

[31] M. Roger, S. Moreau, and A. Guédel, *Broadband fan noise prediction using single-airfoil theory*, Noise Control Engineering Journal **54** (2006), no. 1, 5–14.

[32] Y. Rozenberg, G. Robert, and S. Moreau, *Wall-pressure spectral model including the adverse pressure gradient effects*, AIAA Journal **50** (2012), no. 10, 2168–2179.

[33] M. Sanjosé and S. Moreau, *Fast and accurate analytical modeling of broadband noise for a low-speed fan*, Accepted for publication in the Journal of the Acoustical Society of America, 2018.

[34] R. Schlinker and R. K. Amiet, *Helicopter trailing edge noise.*, Tech. report, NASA, 1981.

[35] M. Slama, C. Leblond, and P. Sagaut, *A kriging-based elliptic extended anisotropic model for the turbulent boundary layer wall pressure spectrum*, Journal of Fluid Mechanics **840** (2018), 25–55.

[36] D. K. Wilson, *Three-dimensional correlation and spectral functions for turbulent velocities in homogeneous and surface-blocked boundary layers*, Tech. report, Army Research Laboratory, July 1997.